AGU PUBLICATIONS

JGR

Journal of Geophysical Research: Space Physics

BRIEF REPORT

10.1002/2013JA019193

**Key Points:**
- The solar wind electric field does not control the dayside reconnection rate
- Rather, the reconnection rate and the sheath flow control the electric fields
- A modification improves electric field drivers but ruins their interpretation

**Correspondence to:**
J. E. Borovsky,
jborovsky@spacescience.org

**Citation:**
Borovsky, J. E., and J. Birn (2014), The solar wind electric field does not control the dayside reconnection rate, *J. Geophys. Res. Space Physics*, *119*, 751–760, doi:10.1002/2013JA019193.

Received 2 JUL 2013
Accepted 12 JAN 2014
Accepted article online 17 JAN 2014
Published online 10 FEB 2014

# The solar wind electric field does not control the dayside reconnection rate

**Joseph E. Borovsky[1,2,3] and Joachim Birn[1]**

[1]Center for Space Plasma Physics, Space Science Institute, Boulder, Colorado, USA, [2]AUSS, University of Michigan, Lansing, Michigan, USA, [3]Department of Physics, Lancaster University, Lancaster, UK

**Abstract** Working toward a physical understanding of how solar wind/magnetosphere coupling works, four arguments are presented indicating that the solar wind electric field $\underline{v}_{sw} \times \underline{B}_{sw}$ does not control the rate of reconnection between the solar wind and the magnetosphere. Those four arguments are (1) that the derived rate of dayside reconnection is not equal to solar wind electric field, (2) that electric field driver functions can be improved by a simple modification that disallows their interpretation as the solar wind electric field, (3) that the electric field in the magnetosheath is not equal to the electric field in the solar wind, and (4) that the magnetosphere can mass load and reduce the dayside reconnection rate without regard for the solar wind electric field. The data are more consistent with a coupling function based on local control of the reconnection rate than the Axford conjecture that reconnection is controlled by boundary conditions irrespective of local parameters. Physical arguments that the solar wind electric field controls dayside reconnection are absent; it is speculated that it is a coincidence that the electric field does so well at correlations with geomagnetic indices.

## 1. Introduction

It is commonly assumed that the value of the solar wind motional electric field $\underline{E}_{sw} = -\underline{v}_{sw} \times \underline{B}_{sw}$ determines the rate of reconnection between the solar wind and the magnetosphere at the dayside magnetopause. It is argued that this solar wind electric field is applied at the dayside magnetopause and that the reconnection electric field on the magnetopause is equal to the applied solar wind electric field. The rate of reconnection is the reconnection electric field. Arguments that $E_{sw}$ can be equated with the dayside reconnection rate appeared in *Gonzalez and Mozer* [1974], *Kan and Lee* [1979], *Gonzalez and Gonzalez* [1981], and *Sergeev and Kuznetsov* [1981], and this concept persists through the decades up to the present time [e.g., *Reiff and Luhmann*, 1986; *Baumjohann and Paschmann*, 1987; *Goertz et al*., 1993; *Vassiliadis et al*., 1999; *Pulkkinen et al*., 2007; *Rothwell and Jasperse*, 2007; *Kan et al*., 2010; *Milan et al*., 2012].

Taking $v_{sw}$ to be the speed of the solar wind plasma (in the Earth's reference frame) and $B_\perp$ to be the transverse-to-radial strength of the interplanetary magnetic field (IMF), solar wind electric field driver functions are written in various forms as $v_{sw}B_\perp$ times a clock angle function [*Wygant et al*., 1983; *Gonzalez*, 1990]. When the solar wind electric field driver functions are cross-correlated with geomagnetic indices, the correlation coefficients are not bad (cf. *Wygant et al*. [1983, Table 2], *Newell et al*. [2007, Table 3], or Table 1).

Contrary to this electric field picture, recent papers have argued that dayside reconnection is controlled by a local picture wherein the local reconnection rate is governed by the local plasma parameters near the reconnection site [*Borovsky et al*., 2008; *Borovsky*, 2008, 2013a, 2013b].

These two pictures (driven by $E_{sw}$ versus controlled by local plasma parameters) are related to the "Axford conjecture" [*Axford*, 1984; *Buchner*, 2007] which posed that reconnection is driven by an electric field boundary condition and is not controlled by local parameters. In the driven picture the reconnection rate is thought to adjust to the electric field on a boundary condition remote from the reconnection site. This view appears to be consistent with 2-D steady models of reconnection, in which the electric field is uniform, such that the reconnection rate is the same as the electric field at the boundary, presumed to be imposed. Contrary to this conjecture, computer simulations of driven reconnection in two dimensions by *Birn and Hesse* [2007] find that the reconnection rate does not in general match the electric field at the boundary condition. The main reason is that the imposed electric field does not stay uniform within the simulation box

**Table 1.** The Linear Correlation Coefficients Between Various Solar Wind Driver Functions and Eight Geomagnetic Indices[a]

| | $AE_1$ | $AU_1$ | $-AL_1$ | $PCI_0$ | $MBI_1$ | $KP_1$ | $ap_1$ | $-Dst_2$ | 8-Index Average |
|---|---|---|---|---|---|---|---|---|---|
| $\sin^2(\theta/2)$ | 0.510 | 0.439 | 0.493 | 0.499 | 0.458 | 0.333 | 0.242 | 0.279 | 0.407 |
| $vB_\perp$ | 0.434 | 0.404 | 0.404 | 0.432 | 0.462 | 0.530 | 0.583 | 0.450 | 0.462 |
| $vB_z$ | 0.575 | 0.451 | 0.578 | 0.580 | 0.470 | 0.346 | 0.391 | 0.384 | 0.472 |
| $vB_{south}$ | 0.688 | 0.543 | 0.689 | 0.656 | 0.606 | 0.534 | 0.629 | 0.558 | 0.613 |
| $vB_\perp\sin^2(\theta/2)$ | 0.708 | 0.600 | 0.688 | 0.712 | 0.657 | 0.618 | 0.687 | 0.587 | 0.657 |
| $vB_\perp\sin^4(\theta/2)$ | 0.718 | 0.584 | 0.709 | 0.703 | 0.646 | 0.585 | 0.670 | 0.586 | 0.650 |
| $v^{4/3}B_\perp{}^{2/3}\sin^{8/3}(\theta/2)$ | 0.775 | 0.645 | 0.759 | 0.757 | 0.710 | 0.649 | 0.669 | 0.596 | 0.695 |
| $R_{quick}$ | 0.761 | 0.660 | 0.732 | 0.749 | 0.723 | 0.692 | 0.708 | 0.594 | 0.702 |

[a]Hourly averaged values from 1963 to 2012 for all quantities are used. The subscript in the name of the index indicates the number of hours of time lag between the value of the index and the time of evaluation of the solar wind parameters going into the driver function.

but gets modified from spatial and temporal variations, such that the field parameters right at the inflow into the reconnection site may differ significantly from the parameters far away.

Supporting this contradiction to the Axford conjecture is the derivation of the Cassak-Shay equation for the local rate of reconnection between asymmetric plasmas written in terms of local plasma parameters [*Cassak and Shay*, 2007; *Birn et al*., 2012]. The Cassak-Shay equation for the reconnection rate $R$ has been tested for magnetic clock angles of 180° in a variety of computer simulations of reconnection with wide ranges of densities and magnetic field strengths [e.g., *Borovsky and Hesse*, 2007; *Borovsky et al*., 2008; *Birn et al*., 2008, 2010; *Malakit et al*., 2010; *Donato et al*., 2012]: For varying clock angles, simulations [*Hesse et al*., 2013] question the clock angle dependence of asymmetric reconnection (cf. section 2.1). The Cassak-Shay formulation has been successfully used to predict the measured reconnection outflow speeds at the magnetopause for a wide range of densities and magnetic field strengths in the magnetosheath and magnetosphere [*Walsh et al*., 2013a, 2013b] at various IMF clock angles. In the symmetric-plasma limit, the Cassak-Shay equation reduces to the familiar Petschek formula for the fast reconnection rate $R \sim 0.1 v_A B$ that has been successfully tested in a variety of computer simulations in the Geospace Environmental Modeling (GEM) reconnection challenge [*Birn et al*., 2001; *Otto*, 2001; *Shay et al*., 2001; *Birn and Hesse*, 2001] and tested against dayside reconnection measurements [*Fuselier et al*., 2010], magnetosheath reconnection measurements [*Phan et al*., 2007], and collisionless plasma laboratory experiments [*Yamada et al*., 2006; *Ren et al*., 2008].

In section 2 this report presents four pieces of evidence that indicate that the solar wind electric field $E_{sw}$ does not control the dayside reconnection rate between the solar wind and the magnetosphere. Those are (1) that the derived local rate of reconnection is not equal to solar wind electric field and the data are more consistent with the derived rate than with the solar wind electric field, (2) that electric field driver functions can be improved with a modification that disallows their interpretation as the solar wind electric field, (3) that the electric field in the magnetosheath is not equal to the electric field in the solar wind, and (4) that the magnetosphere can mass load the dayside reconnection rate without regard to the solar wind electric field. The report is summarized in section 3, which also contains discussions about dayside reconnection and the solar wind electric field.

## 2. Indications That the Solar Wind Electric Field $E_{sw}$ Does not Control the Dayside Reconnection Rate

Four indications that the solar wind electric field is not the controller of the dayside reconnection rate between the solar wind and the magnetosphere are given below.

### 2.1. The Derived Rate of Reconnection is not the Solar Wind Electric Field

In this subsection the dayside local reconnection rate between the solar wind and the magnetosphere will be derived from the well-tested Cassak-Shay equation for the rate of reconnection $R$ between two plasmas with asymmetric properties. Labeling these two plasmas with subscripts "1" and "2," the Cassak-Shay equation is

$$R = \left(0.2/\mu_o{}^{1/2}\right)\sin^2(\theta/2)B_1{}^{3/2}B_2{}^{3/2}/\left\{(B_1\rho_2 + B_2\rho_1)^{1/2}(B_1 + B_2)^{1/2}\right\} \quad (1)$$

[*Cassak and Shay*, 2007; *Birn et al*., 2008, 2010], where $B_1$ and $B_2$ are the magnetic field strengths in plasmas 1 and 2, and $\rho_1$ and $\rho_2$ are the mass densities of plasmas 1 and 2. In expression (1) the *Sonnerup* [1974] $\sin^2(\theta/2)$

clock angle dependence of the reconnection rate has been included, where $\theta$ is the angle between the magnetic field direction in plasma 1 and the magnetic field direction in plasma 2. There is controversy as to the actual physical form of the clock angle dependence of the asymmetric-plasma reconnection rate [cf. *Swisdak and Drake*, 2007; *Borovsky*, 2013a; *Hesse et al*., 2013], but all forms are close to $\sin^2(\theta/2)$.

If plasmas 1 and 2 are symmetric (with $B_1 = B_2$ and $\rho_1 = \rho_2$) then expression (1) simplifies to the familiar $R = 0.1 \sin^2(\theta/2)\, v_A B$, where $v_A = B/(\mu_o \rho)^{1/2}$ is the Alfvén speed in either plasma and $B$ is the magnetic field strength in either plasma. If plasmas 1 and 2 are very asymmetric, then expression (1) simplifies to

$$R = \ 0.2 \sin^2(\theta/2)\, v_{A\,\mathrm{slow}} (B_{\mathrm{fast}}\, B_{\mathrm{slow}})^{1/2} \tag{2}$$

where the subscripts "fast" and "slow" refer to the plasma with the faster Alfvén speed and the plasma with the slower Alfvén speed, respectively. For the magnetosheath and the dayside magnetosphere, the magnetosphere almost always has the faster Alfvén speed. For a "quick" derivation of the local dayside reconnection rate $R$ at the nose of the magnetosphere, expression (2) will be used and the fast plasma will be taken to be the magnetosphere with subscript "$m$" and the slow plasma will be taken to be the magnetosheath with subscript "$s$". Expression (2) then becomes

$$R = 0.2 \left(\mu_o m_p\right)^{-1/2} \sin^2(\theta/2) B_s^{3/2} B_m^{1/2} n_s^{-1/2} \tag{3}$$

The methodology of *Borovsky* [2008, 2013a] can be used to express $B_s$, $B_m$, and $n_s$ in terms of upstream solar wind parameters. Pressure balance between the magnetosphere and the solar wind gives [cf. *Borovsky*, 2008, equation (4)]

$$B_m = \left(2\mu_o m_p\right)^{1/2} n_{\mathrm{sw}}^{1/2} v_{\mathrm{sw}} \tag{4}$$

pressure balance between the magnetosheath and the magnetosphere gives [cf. *Borovsky*, 2008, equation (5)]

$$B_s = B_m (1+\beta_s)^{-1/2} = \left(2\mu_o m_p\right)^{1/2} n_{\mathrm{sw}}^{1/2} v_{\mathrm{sw}} (1+\beta_s)^{-1/2} \tag{5}$$

where $\beta_s = 2\mu_o n_s k_B T_s / B_s^2$ is the plasma beta of the magnetosheath. Two parameterizations obtained from multiple MHD simulations are [cf. *Borovsky*, 2008, equations (9) and (7)]

$$n_s = C\, n_{\mathrm{sw}} \tag{6a}$$

$$\beta_s = (M_A/6)^{1.92} \tag{6b}$$

where $C$ is the compression ratio of the bow shock and $M_A = v_{\mathrm{sw}} (\mu_o m_p n_{\mathrm{sw}})^{1/2} / B_{\mathrm{sw}}$ is the Alfvén Mach number of the upstream solar wind. The compression ratio $C$ can be expressed as [cf. *Borovsky*, 2008, equation (10)]

$$C = \left\{ 2.44 \times 10^{-4} + [1 + 1.38 \log_e(M_A)]^{-6} \right\}^{-1/6} \tag{7}$$

Using expressions (4)–(7), expression (3) becomes the quick derivation

$$R_{\mathrm{quick}} = 0.4 \mu_o^{1/2} m_p^{1/2} \sin^2(\theta/2)\, C^{-1/2} n_{\mathrm{sw}}^{1/2} v_{\mathrm{sw}}^2 (1+\beta_s)^{-3/4} \tag{8}$$

for the dayside reconnection rate at the nose of the magnetosphere. In expression (8) $C$ and $\beta_s$ are functions of the Alfvén Mach number, which has the dependence $M_A \propto v_{\mathrm{sw}} n_{\mathrm{sw}}^{1/2} B_{\mathrm{sw}}^{-1}$. Hence, $R_{\mathrm{quick}}$ is a function of four upstream-solar wind parameters: $\theta$, $n_{\mathrm{sw}}$, $v_{\mathrm{sw}}$, and $B_{\mathrm{sw}}$ (where $B_{\mathrm{sw}} = (B_x^2 + B_y^2 + B_z^2)^{1/2}$ is the magnitude of the field in the solar wind).

To evaluate the function $R_{\mathrm{quick}}$ for the dayside local reconnection rate, geomagnetic indices are used. Geomagnetic indices are measures of various forms of geomagnetic activity (magnetospheric convection, strengths of current systems, and plasma diamagnetism), which are responding to the total rate of dayside reconnection but are not direct measures of the reconnection rate. (In *Borovsky* [2013b] a line of research to derive a solar wind driver function for the total dayside reconnection rate is described: Similar correlations with geomagnetic indices are obtained for local drivers and total drivers.) A more direct measure of the local reconnection rate would be the ionospheric electric field along the dayside open-closed boundary [*Baker et al*., 1997; *Chisham et al*., 2004, 2008], and a more direct measure of the total reconnection rate would be the dayside contribution to the cross-polar cap potential [*Lockwood et al*., 1990, 2005; *Milan et al*., 2012]. However, large databases of such direct measurements are not available.

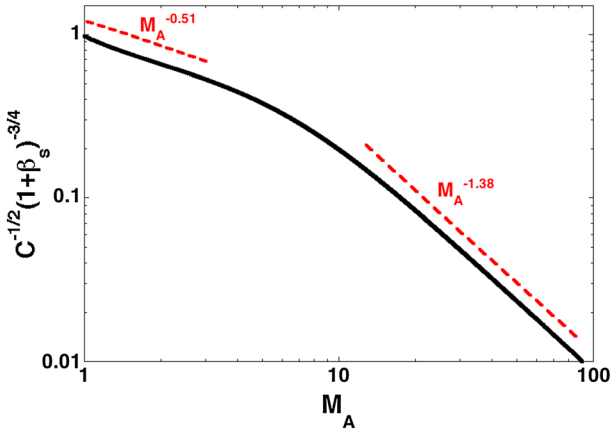


**Figure 1.** The Alfvén Mach number dependence of the quantity $C^{-1/2}(1+\beta_s)^{-3/4}$ in $R_{quick}$ (expression (8)) is plotted. The functional forms of fits to $C^{-1/2}(1+\beta_s)^{-3/4}$ at low and high Mach number are indicated by the red dashed curves.

The Pearson linear correlation coefficients [*Bevington and Robinson*, 1992, equation (11.17)] between $R_{quick}$ evaluated with hourly averaged solar wind parameters $\theta$, $n_{sw}$, $v_{sw}$, and $B_{sw}$ from OMNI2 [*King and Papitashvili*, 2005] and hourly values of eight geomagnetic indices are listed in Table 1. Also listed are the linear correlation coefficients for several solar wind electric field driver functions. The OMNI2 data from 1963 to 2012 is used, comprising 288,040 h of plasma and magnetic field measurements. Uncertainties in the correlation coefficients are in the third decimal place. As can be seen in Table 1, the quick derivation $R_{quick}$ for the local reconnection rate does a very good job of correlating with geomagnetic indices; for the 8-index average of the correlation coefficients it does better than all of the various electric field functions.

In Figure 1 the Alfvén Mach number dependence of $C^{-1/2}(1+\beta_s)^{-3/4}$ in expression (8) is plotted. As can be seen, there is a transition in the Mach number dependence at about $M_A \sim 6$: This is the division between low-beta magnetosheath flow for $M_A < 6$ and high-beta magnetosheath flow for $M_A > 6$ (cf. expression (6b)). As indicated in red in Figure 1, the Mach number dependence of $C^{-1/2}(1+\beta_s)^{-3/4}$ can be fit at low Mach number as $C^{-1/2}(1+\beta_s)^{-3/4} \propto {M_A}^{-0.51} \propto {v_{sw}}^{-0.51}{n_{sw}}^{-0.26}{B_{sw}}^{0.51}$ and the Mach number dependence of $C^{-1/2}(1+\beta_s)^{-3/4}$ can be fit at high Mach number as $C^{-1/2}(1+\beta_s)^{-3/4} \propto {M_A}^{-1.38} \propto {v_{sw}}^{-1.38}{n_{sw}}^{-0.69}{B_{sw}}^{1.38}$. Using these scalings for $C^{-1/2}(1+\beta_s)^{-3/4}$ in expression (8) at low and high Mach numbers, the functional form of $R_{quick}$ is

$$R_{quick} \propto \sin^2(\theta/2)\, {n_{sw}}^{0.24}{v_{sw}}^{1.49}{B_{sw}}^{0.51} \quad \text{at low } M_A \tag{9a}$$

$$R_{quick} \propto \sin^2(\theta/2)\, {n_{sw}}^{-0.19}{v_{sw}}^{0.62}{B_{sw}}^{1.38} \quad \text{at high } M_A \tag{9b}$$

Although the functional form of $R_{quick}$ in expressions (9a) and (9b) resembles the functional form of the solar wind's motional electric field $E_{sw} \sim vB_\perp$, $R_{quick}$ is not the electric field. In the derivation the $v_{sw}$ in expressions (8) and (9) comes from (1) the ram pressure of the solar wind which determines the magnetic field strength at the nose of the magnetosphere, (2) the Alfvén Mach number of the solar wind determining the plasma beta of the magnetosheath which in turn determines the magnetic field strength in the magnetosheath, and (3) the Alfvén Mach number of the solar wind determining the compression ratio of the bow shock which in turn determines the density of the magnetosheath plasma. Further, in expressions (9a) and (9b) $B_{sw}$ is $B_{mag} = (B_x^2 + B_y^2 + B_z^2)^{1/2}$, not the $B_\perp = (B_y^2 + B_z^2)^{1/2}$ of the solar wind electric field.

To summarize this subsection, the data are more consistent with a coupling function based on local control of the reconnection rate than the Axford conjecture.

### 2.2. Electric Field Driver Functions can be Improved by Replacing $B_\perp$ With $B_{mag}$

The functional forms of $R_{quick}$ in expressions (9a) and (9b) resemble the functional form of the solar wind electric field which goes as $v_{sw}B_\perp$, but with $B_{mag} = (B_x^2 + B_y^2 + B_z^2)^{1/2}$ of the upstream solar wind instead of $B_\perp = (B_y^2 + B_z^2)^{1/2}$ of the upstream solar wind. In fact, for traditional electric field driver functions, replacing $B_\perp$ by $B_{mag}$ in general improves their correlations with geomagnetic indices. This is demonstrated in Table 2 where the driver functions $v_{sw}B_\perp$ (which is the solar wind electric field $E_\perp$), $v_{sw}B_\perp\sin^2(\theta/2)$ [*Kan and Lee*, 1979], $v_{sw}B_\perp\sin^4(\theta/2)$ [*Wygant et al.*, 1983], and ${v_{sw}}^{4/3}{B_\perp}^{2/3}\sin^{8/3}(\theta/2)$ [*Newell et al.*, 2007] are each modified by replacing $B_\perp$ by $B_{mag}$ and then the correlations with geomagnetic indices are compared for the original and the modified functions. In the second column of Table 2 the functional forms of the original and modified functions are listed. In the third column the average of the Pearson linear correlation coefficient of the function with eight geomagnetic indices (cf. Table 1) is listed. In the final column of Table 2 the "improvement factor" obtained by modifying the original function is listed, where the improvement factor is the 8-index-average correlation coefficient for the

**Table 2.** For Four Solar Wind Electric Field Functions, the Functions Are Modified by Replacing $B_\perp$ With $B_{mag}$ (of the Solar Wind) and Then the Linear Correlation Coefficients Between Geomagnetic Indices and the Original and Modified Functions Are Compared[a]

| Electric Field Function | Functional Form | 8-Index Average | Improvement Factor |
|---|---|---|---|
| $E_\perp$ | $vB_\perp$ | 0.462 | 1.15 |
| | $vB_{mag}$ | 0.533 | |
| Kan + Lee | $vB_\perp \sin^2(\theta/2)$ | 0.657 | 1.06 |
| | $vB_{mag}\sin^2(\theta/2)$ | 0.694 | |
| Wygant | $vB_\perp \sin^4(\theta/2)$ | 0.650 | 1.02 |
| | $vB_{mag}\sin^4(\theta/2)$ | 0.664 | |
| Newell | $v^{4/3}B_\perp{}^{2/3}\sin^{8/3}(\theta/2)$ | 0.695 | 0.99 |
| | $v^{4/3}B_{mag}{}^{2/3}\sin^{8/3}(\theta/2)$ | 0.686 | |

[a]Measurements from 1963 to 2012 are utilized.

modified function divided by the 8-index-average correlation coefficient for the original electric field function. Except for the Newell function, replacing $B_\perp$ by $B_{mag}$ in the electric field function improves its performance. The Newell function shows a slight (1%) decrease in performance against the geomagnetic indices; however, if the modified function $v_{sw}{}^{4/3}B_\perp{}^{1/3}B_{mag}{}^{1/3}\sin^{8/3}(\theta/2)$ is used, a 1% improvement over the original Newell function is obtained.

It can be conjectured that is a matter of luck that the solar wind electric field correlates so well with geomagnetic indices. This improvement of the electric field driver functions by replacing $B_\perp$ with $B_{mag}$ indicates that better luck would have been obtained by guessing $v_{sw}B_{mag}$ rather than $v_{sw}B_\perp$.

### 2.3. The Motional Electric Field is Modified in the Magnetosheath Flow Pattern

As noted in section 1, it has been argued in the literature that the solar wind electric field applied at the magnetopause determines the reconnection (merging) electric field. However, owing to the compression and deflection of the plasma flow across the bow shock and to the divergence and shear of the flow in the magnetosheath, the electric field in the magnetosheath is not equal to the electric field $E_{sw}$ in the upstream solar wind: At some locations in the magnetosheath it is weaker than $E_{sw}$, and at other locations in the magnetosheath it is stronger than $E_{sw}$.

The electric field pattern in the magnetosheath depends on the Mach number of the solar wind flow past the Earth. This is demonstrated in Figure 2 (left and right) where the dawn-dusk component of the electric field $E_y$ is plotted in color in the equatorial plane for two global-MHD simulations of the solar wind flow past the Earth, one for higher Alfvén Mach number (Figure 2, left) and one for lower Alfvén Mach number (Figure 2, right).

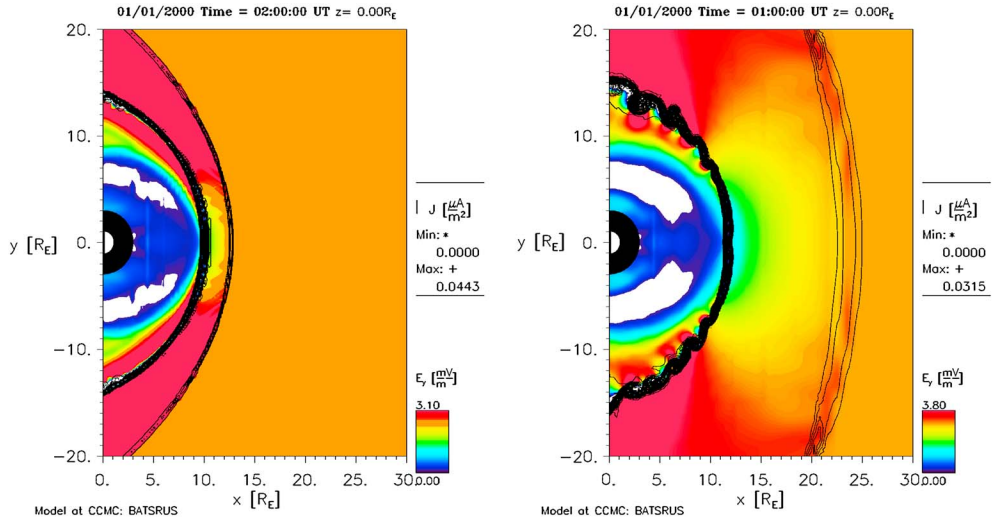


**Figure 2.** Equatorial-plane cuts from two global-MHD simulations of the flow of the solar wind past the Earth performed with the BATSRUS simulation code are displayed. (left) The runs are "Joe_Borovsky_040207_1f" with a Mach number $M_A = 8.2$ and (right) "Joe_Borovsky_050807_4" with a Mach number $M_A = 1.95$. In Figure 2 (left and right) the electric field $E_y$ is plotted in color with total current density $j = (j_x{}^2 + j_y{}^2 + j_z{}^2)^{1/2}$ plotted as the black contours to highlight the bow shock and magnetopause.

The simulations were performed with the Block-Adaptive-Tree-Solarwind-Roe-Upwind-Scheme (BATSRUS) simulation code [*De Zeeuw et al.*, 2000; *Gombosi et al.*, 2000] at the Community Coordinated Modeling Center [*Rastatter et al.*, 2012]. The Sun is off to the right in Figure 2 (left and right), and the color scales are adjusted so that $E_y$ of the unshocked solar wind is orange. The black contours highlight the bow shock and the magnetopause. In both simulations the IMF clock angle is $\theta = 180°$ (purely southward IMF), and dayside reconnection is ongoing. The resistive-spot method [cf. *Borovsky et al.*, 2008, Appendix A; *Birn et al.*, 2008] is utilized in both simulations to ensure that the reconnection rate in the MHD simulations correctly emulates the collisionless plasma Petschek fast rate [*Borovsky et al.*, 2008, 2009] obtained in Hall-MHD, hybrid, and full-particle simulations as part of the GEM reconnection challenge study [*Birn et al.*, 2001]. Note in Figure 2 (left) at high Mach number (where the shock standoff distance is at $x \sim 12\ R_E$) that the magnetosheath is narrow and in Figure 2 (right) at low Mach number (where the shock standoff distance is at $x \sim 23\ R_E$) that the magnetosheath is wide. Note in Figure 2 (left and right) that $E_y$ decreases along the Sun-Earth line in going from the unshocked solar wind through the magnetosheath toward the magnetopause. In Figure 2 (left and right) it can be seen that the spatial pattern in the magnetosheath of reduction and enhancement of the electric field depends on the Mach number of the solar wind flow. The electric field in the magnetosheath is not equal to the electric field in the solar wind (see also *Borovsky et al.* [2008, Figure 6]).

It is instructive to identify the physical signatures of the regions where the electric field becomes modified. In general, any vector field can be inferred from its sources of curl and divergence. (This is a consistency analysis and not an assignment of cause and effect.) In a steady state flow around the magnetosphere, $\partial/\partial t = 0$, so Faraday's law yields $\nabla \times \underline{E} = 0$. In that case modifications of the electric field in the flowing plasma are determined by Coulomb's law $\nabla \cdot \underline{E} = \rho_q/\varepsilon_o$ where $\rho_q$ is the net charge density in the plasma. For frozen-in flow with $\underline{E} = -\underline{v} \times \underline{B}$, Coulomb's law $\nabla \cdot (-\underline{v} \times \underline{B}) = \rho_q/\varepsilon_o$ becomes

$$-\underline{B} \cdot \left( \nabla \times \underline{v} \right) + \underline{v} \cdot \left( \nabla \times \underline{B} \right) = \rho_q/\varepsilon_o \tag{10}$$

Using the definition of vorticity $\omega \equiv \nabla \times \underline{v}$ and using Ampere's law (with zero displacement current) $\nabla \times \underline{B} = \mu_o \underline{j}$, expression (10) becomes

$$\rho_q/\varepsilon_o = -\underline{\omega} \cdot \underline{B} + \mu_o \underline{v} \cdot \underline{j} \tag{11}$$

for the source of electric field $\rho_q/\varepsilon_o$ in Coulomb's law. In the plasma flow, charge density is associated with vorticity $\omega$ [cf. *Seyler et al.*, 1975; *Borovsky and Hansen*, 1998], where $\omega \cdot \underline{B}$ is a gradient of the flow across the magnetic field. The term $\mu_o \underline{v} \cdot \underline{j}$, which is a gradient of the magnetic field across the flow, is the nonrelativistic motional transformation of current density into charge density [cf. *Podolsky*, 1947] that goes with the motional transformation of magnetic field into electric field ($\underline{E} = -\underline{v} \times \underline{B}$). Hence, the electric field in the magnetosheath MHD flow is modified at the locations where $\omega \cdot \underline{B} \neq 0$ and where $\underline{v} \cdot \underline{j} \neq 0$. For $\omega \cdot \underline{B}$, these locations are the abrupt vorticity layers of the bow shock and the magnetopause and the large-scale velocity shear in the magnetosheath flow pattern. For $\underline{v} \cdot \underline{j}$, these locations are the oblique portions of the bow shock and the bulk flow of the compressed magnetosheath. The magnetosheath electric field with its source $\nabla \cdot \underline{E}$ in these regions can be seen in the three panels of Figure 3. In Figure 3 (left) the total electric field strength is plotted in color along with the electric field vectors in black for the flow of the solar wind through the bow shock and around the magnetosphere from the same simulation as Figure 2 (left). The location of the bow shock and the magnetopause are highlighted in Figure 3 (left) by the black contours of constant current density $|\underline{j}|$. The electric field vectors in Figure 3 (left) indicate the nonzero divergence of $\underline{E}$ at the bow shock, at the magnetopause, and within the sheared magnetosheath. In Figure 3 (middle) the value of $\underline{v} \cdot \underline{j}$ calculated in the MHD simulation is plotted in color; as can be seen, $\underline{v} \cdot \underline{j}$, which is a location of nonzero charge density in the plasma, is strong at the magnetopause and at the bow shock. In Figure 3 (right) the value of $\omega \cdot \underline{B}$ calculated in the MHD simulation is plotted in color; as can be seen, $\omega \cdot \underline{B}$, which is a location of nonzero charge density in the plasma, is strong at the magnetopause.

As depicted in Figures 2 and 3, the flow-controlled electric field in the plasma around the Earth is greatly modified from the upstream solar wind value by the Mach number dependent locations of the bow shock and the Mach number dependent shear pattern of the magnetosheath flow between the magnetopause and the bow shock.

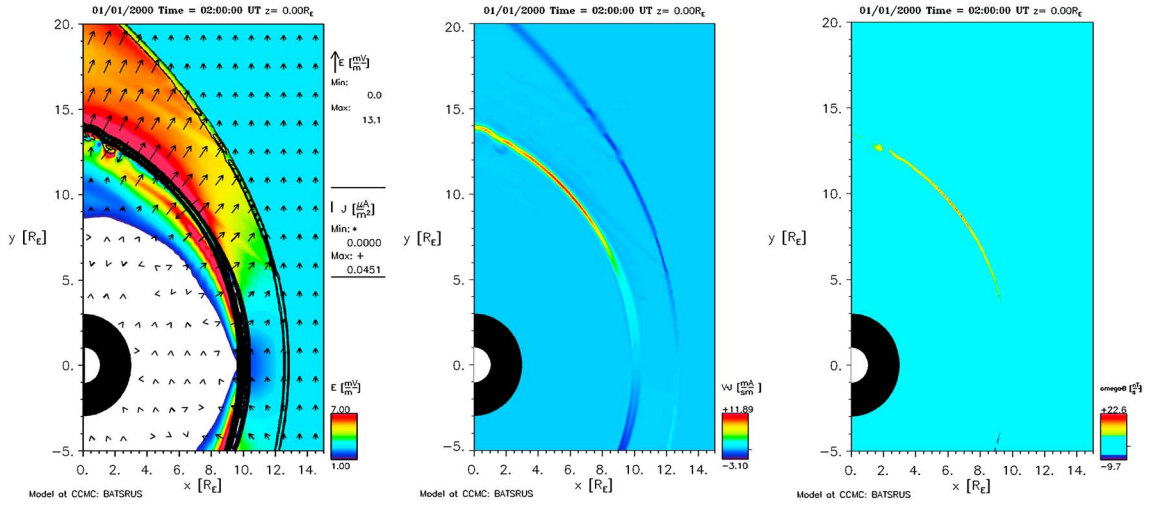


**Figure 3.** Three equatorial-plane cuts from the global-MHD simulation "Joe_Borovsky_040207_1f" with a Mach number $M_A = 8.2$. (left) The magnitude of the electric field $E$ is plotted in color, the electric field vectors are plotted as the black arrows, and the total current density $j = (j_x^2 + j_y^2 + j_z^2)^{1/2}$ plotted as the black contours to highlight the bow shock and magnetopause. (middle) The quantity $\underline{v} \cdot \underline{j}$ in the flow is plotted, and (right) the quantity $\omega \cdot \underline{B}$ in the flow is plotted.

### 2.4. Magnetospheric Mass Loading Changes the Reconnection Rate Without Regard to $E_{sw}$

The Cassak-Shay equation predicts, and global-MHD simulations show, that mass loading by dense magnetospheric plasma can reduce the dayside reconnection rate. This reduction in the reconnection rate is independent of the value of $E_{sw}$. In a global-MHD simulation with a purely southward IMF, the local reconnection rate across the dayside magnetosphere is plotted as a function of distance from the Sun-Earth line ($y = 0$) in Figure 4. To ensure that the MHD simulations emulate reconnection in a collisionless plasma, the resistive-spot method [cf. *Borovsky et al.*, 2008, Appendix A] is again used in the BATSRUS code. The resistive spot in the 3-D BATSRUS simulation domain is really a resistive cord that temporally flexes to remain along the magnetopause reconnection $X$ line across the dayside magnetosphere. In Figure 4 the electric field $E_{X\ \mathrm{line}}$ along the reconnection $X$ line is normalized to the electric field $E_y$ in the solar wind: $E_{sw} = v_{sw}B_z$. The blue curve is the local reconnection rate at a time in the simulation when the magnetospheric plasma near the magnetopause has a mass density much lower than the mass density of the magnetosheath plasma near the magnetopause. The reconnection rate profile is maximum at the nose of the magnetosphere ($y = 0$) and falls off away from the nose. The red curve in Figure 4 is the local reconnection rate at a time when a high-density plume of magnetospheric plasma is flowing into the reconnection $X$ line at the nose. As can be seen, the reconnection rate is locally reduced by this dense plume at the nose: The rate is not maintained by $E_{sw}$. In *Borovsky et al.* [2008] the Cassak-Shay equation (expression (1)) was evaluated for the properties of the magnetosheath plasma and magnetospheric plasma at the nose, and agreement was found with the measured reconnection rate in the simulation. This is a success for the local-control picture of reconnection and a contradiction for the solar wind electric field-driven reconnection picture.

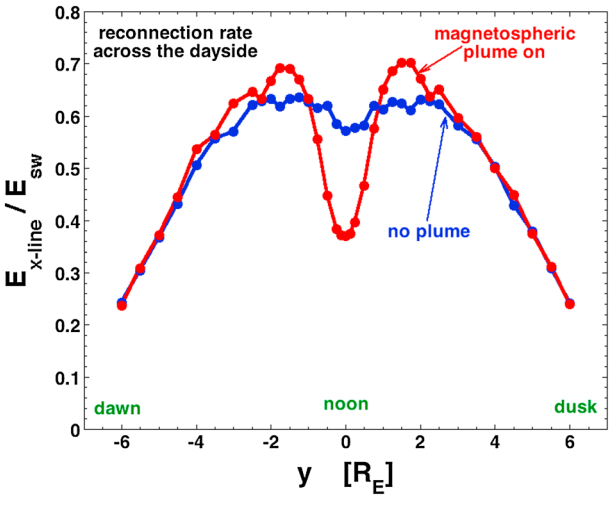


**Figure 4.** The reconnection rate across the dayside magnetosphere is plotted as a function of the dawn-dusk coordinated at two instants of time in a purely southward IMF BATSRUS global-MHD simulation (run "Joe_Borovsky_040207_1f" at the CCMC). The reconnection rate in the simulation is measured as $\eta j$, where $\eta$ is the resistivity of the resistive cord along the $X$ line and $j$ is the current along the $X$ line.

## 3. Summary and Discussion

To summarize, four arguments were presented in section 2 indicating that the solar wind motional electric field $v_{sw}B_{\perp}$ does not control the rate of reconnection between the solar wind and the magnetosphere at the dayside magnetopause. The author knows of no physical argument or calculation indicating that the solar wind electric field does determine the reconnection rate.

On the contrary, the local reconnection rate $R$ controls the tangential electric field in the magnetosheath near the magnetopause. In the flow of the solar wind plasma around the magnetosphere, the reconnection rate $R$ sets the flow boundary condition for the solar wind plasma at the magnetopause. The tangential electric field along the magnetopause is controlled by whether or not there is flow into the magnetopause. If there is no reconnection (i.e., northward IMF), there is no flow into the magnetopause, and there is no magnetopause tangential electric field. If there is reconnection, then the tangential electric field at the magnetopause is determined by the inflow rate into the reconnection site; in the Petschek dynamical picture of fast reconnection [*Parker*, 1979; *Liu et al*., 2012], the reconnection flow is driven by the magnetic tension released by reconnection, which drives the reconnection outflow jet, which by mass conservation drives the reconnection inflow rate. (Indeed, if the reconnection outflow jet is impeded, the reconnection inflow and the reconnection rate are reduced [*Birn et al*., 2009].) The velocity of the reconnection outflow jet is determined by the magnetic field strength in the two reconnecting plasmas and by the mass densities of the two reconnecting plasmas.

The solar wind electric field is the rate at which magnetic flux is carried in the solar wind toward the Earth. The reconnection rate at the magnetopause is not forced by the rate of flow of magnetic flux in the solar wind toward the magnetosphere: The plasma (and the magnetic flux it carries) is free to flow around the magnetosphere, as it does under northward IMF when there is no reconnection.

The solar wind electric field is not the physical driver of dayside reconnection. There is a degree of luck in the fact that solar wind electric field functions $v_{sw}B_{\perp}$ (times a clock angle function) perform so well in correlating with geomagnetic indices. The derivation in section 2.1 implies that it is more or less coincidental that $v_{sw}B_{\perp}$ works. A better job of correlating is done if a derived reconnection driver function is used in the place of electric field functions (cf. Table 1). And, as shown in Table 2, electric field functions can be improved simply by replacing $B_{\perp}$ with $B_{mag}$ for the upstream solar wind (cf. section 2.2), destroying their electric field interpretation.

For Earth's magnetosphere, the method to determine the dayside reconnection rate $R$ from upstream solar wind parameters is to solve the supersonic flow problem of the solar wind around the Earth to determine plasma parameters near magnetopause: Those parameters control the reconnection rate (cf. the Cassak-Shay equation).

Note that in the full solar wind/magnetosphere coupling problem, the solar wind electric field $E_{sw} = v_{sw}B_{\perp}$ may enter post reconnection: The penetration of the solar wind electric field along the magnetic field lines after the solar wind field lines become connected to the Earth's polar cap may be an important aspect of driving geomagnetic currents [e.g., *Goertz et al*., 1993; *Kelley et al*., 2003; *Ridley*, 2007; *Borovsky*, 2013b]. Hence, $E_{sw}$ may be a measure of the strength of the MHD generator after it becomes coupled to the Earth (rather than a controller of the dayside reconnection rate).

**Acknowledgments**
The authors wish to thank Paul Cassak and Bob McPherron for useful conversations and to thank Lutz Rastatter for help. All simulations were performed at the Community Coordinated Modeling Center at NASA/Goddard Space Flight Center. This work was supported at Space Science Institute by the NASA CCMSM-24 Program, the NSF GEM Program, the NASA Magnetospheric Guest Investigators Program, and the NASA Geospace SR&T Program, at the University of Michigan by the NASA Geospace SR&T Program, and at the University of Lancaster by Science and Technology Funding Council grant ST/I000801/1.

Philippa Browning thanks the reviewers for their assistance in evaluating this paper.

## References

Axford, I. (1984), Driven and non-driven reconnection: Boundary conditions, in *Magnetic Reconnection in Space and Laboratory Plasmas*, edited by E. W. Hones, pp. 360, AGU, Washington, D. C.

Baker, K. B., A. S. Rodger, and G. Lu (1997), HF-radar observations of the dayside magnetic merging rate: A Geospace Environment Modeling boundary layer campaign study, *J. Geophys. Res.*, *102*, 9603–9617.

Baumjohann, W., and G. Paschmann (1987), Solar wind-magnetosphere coupling: Processes and observations, *Phys. Scr.*, *T18*, 61–103.

Bevington, P. R., and D. K. Robinson (1992), *Data Reduction and Error Analysis for the Physical Sciences*, 2nd ed., McGraw-Hill, New York.

Birn, J., and M. Hesse (2001), Geospace Environment Modeling (GEM) magnetic reconnection challenge: Resistive tearing, anisotropic pressure and Hall effects, *J. Geophys. Res.*, *106*, 3737–3750.

Birn, J., and M. Hesse (2007), Reconnection rates in driven magnetic reconnection, *Phys. Plasmas*, *14*, 082306, doi:10.1063/1.2752510.

Birn, J., et al. (2001), Geospace Environment Modeling (GEM) magnetic reconnection challenge, *J. Geophys. Res.*, *106*, 3715–3720.

Birn, J., J. E. Borovsky, and M. Hesse (2008), Properties of asymmetric magnetic reconnection, *Phys. Plasmas*, *15*, 032,101, doi:10.1063/1.2888491.

Birn, J., L. Fletcher, M. Hesse, and T. Neukirch (2009), Energy release and transfer in solar flares: Simulations of three dimensional reconnection, *Astropys. J.*, *695*, 1151–1162.

Birn, J., J. E. Borovsky, M. Hesse, and K. Schindler (2010), Scaling of asymmetric reconnection in compressible plasmas, *Phys. Plasmas*, *17*, 052108.

Birn, J., J. E. Borovsky, and M. Hesse (2012), The role of compressibility in energy release by magnetic reconnection, *Phys. Plasmas*, *19*, 082109.
Borovsky, J. E. (2008), The rudiments of a theory of solar-wind/magnetosphere coupling derived from first principles, *J. Geophys. Res.*, *113*, A08228, doi:10.1029/2007JA012646.
Borovsky, J. E. (2013a), Physical improvements to the solar-wind reconnection control function for the Earth's magnetosphere, *J. Geophys. Res. Space Physics*, *118*, 2113–2121, doi:10.1002/jgra.50110.
Borovsky, J. E. (2013b), Physics based solar-wind driver functions for the magnetosphere: Combining the reconnection-coupled MHD generator with the viscous interaction, *J. Geophys. Res. Space Physics*, *118*, 7119–7150, doi:10.1002/jgra.50557.
Borovsky, J. E., and P. J. Hansen (1998), The morphological evolution and internal convection of ExB-drifting plasma clouds: Theory, dielectric-in-cell simulations, and N-body dielectric simulations, *Phys. Plasmas*, *5*, 3195.
Borovsky, J. E., and M. Hesse (2007), The reconnection of magnetic fields between plasmas with different densities: Scaling relations, *Phys. Plasmas*, *14*, 102,309.
Borovsky, J. E., M. Hesse, J. Birn, and M. M. Kuznetsova (2008), What determines the reconnection rate at the dayside magnetosphere?, *J. Geophys. Res.*, *113*, A07210, doi:10.1029/2007JA012645.
Borovsky, J. E., B. Lavraud, and M. M. Kuznetsova (2009), Polar cap potential saturation, dayside reconnection, and changes to the magnetosphere, *J. Geophys. Res.*, *114*, A03224, doi:10.1029/2009JA014058.
Buchner, J. (2007), Astrophysical reconnection and collisionless dissipation, *Plasma Phys. Control. Fusion*, *49*, B235, doi:10.1088/0741-3335/49/12B/S30.
Cassak, P. A., and M. A. Shay (2007), Scaling of asymmetric magnetic reconnection: General theory and collisional simulations, *Phys. Plasmas*, *14*, 102,114.
Chisham, G., M. P. Freeman, I. J. Coleman, M. Pinnock, M. R. Hairston, M. Lester, and G. Sofko (2004), Measuring the dayside reconnection rate during an interval of due northward interplanetary magnetic field, *Ann. Geophys.*, *22*, 4243–4258.
Chisham, G., et al. (2008), Remote sensing of the spatial and temporal structure of magnetopause and magnetotail reconnection from the ionosphere, *Rev. Geophys.*, *46*, RG1004, doi:10.1029/2007RG000223.
De Zeeuw, D. L., T. I. Gombosi, C. P. T. Groth, K. G. Powell, and Q. F. Stout (2000), An adaptive MHD method for global space weather simulations, *IEEE Trans. Plasma Sci.*, *28*, 1956–1965.
Donato, S., S. Servidio, P. Mitruk, M. A. Shay, P. A. Cassak, and W. H. Matthaeus (2012), Reconnection events in two-dimensional Hall magnetohydrodynamic turbulence, *Phys. Plasmas*, *19*, 092,307–092,309.
Fuselier, S. A., S. M. Petrinic, and K. J. Trattner (2010), Antiparallel magnetic reconnection rates at the Earth's magnetopause, *J. Geophys. Res.*, *115*, A01207, doi:10.1029/2010JA015302.
Goertz, C. K., L.-H. Shan, and R. A. Smith (1993), Prediction of geomagnetic activity, *J. Geophys. Res.*, *98*, 7673–7684.
Gombosi, T. I., D. L. De Zeeuw, C. P. T. Groth, and K. G. Powell (2000), Magnetospheric configuration for Parker-spiral IMF conditions: Results of a 3D AMR MHD simulation, *Adv. Space Res.*, *26*, 139–149.
Gonzalez, W. D. (1990), A unified view of solar wind-magnetosphere coupling functions, *Planet. Space Sci.*, *38*, 627–632.
Gonzalez, W. D., and A. L. C. Gonzalez (1981), Solar wind energy and electric field transfer to the Earth's magnetosphere via magnetopause reconnection, *Geophys. Res. Lett.*, *8*, 265–268.
Gonzalez, W. D., and F. S. Mozer (1974), A quantitative model for the potential resulting from reconnection with an arbitrary interplanetary magnetic field, *J. Geophys. Res.*, *79*, 4186–4194.
Hesse, M., N. Aunai, S. Zenitani, M. Kuznetsova, and J. Birn (2013), Aspects of collisionless magnetic reconnection in asymmetric systems, *Phys. Plasmas*, *20*, 061,210.
Kan, J. R., and L. C. Lee (1979), Energy coupling function and solar wind-magnetosphere dynamo, *Geophys. Res. Lett.*, *6*, 577–580.
Kan, J. R., H. Li, C. Wang, B. B. Tang, and Y. Q. Hu (2010), Saturation of polar cap potential: Nonlinearity in quasi-steady solar wind-magnetosphere-ionosphere coupling, *J. Geophys. Res.*, *115*, A08226, doi:10.1029/2009JA014389.
Kelley, M. C., J. J. Makela, J. L. Chau, and M. J. Nicolls (2003), Penetration of the solar wind electric field into the magnetosphere/ionosphere system, *Geophys. Res. Lett.*, *30*(41158), doi:10.1029/2002GL016321.
King, J. H., and N. E. Papitashvili (2005), Solar wind spatial scales in and comparisons of hourly Wind and ACE plasma and magnetic field data, *J. Geophys. Res.*, *110*, A02104, doi:10.1029/2004JA010649.
Liu, Y. H., J. F. Drake, and M. Swisdak (2012), The structure of the magnetic reconnection exhaust boundary, *Phys. Plasmas*, *19*, 022,110.
Lockwood, M., S. W. H. Cowley, and M. P. Freeman (1990), The excitation of plasma convection in the high-latitude ionosphere, *J. Geophys. Res.*, *95*, 7691–7972.
Lockwood, M., J. A. Davies, J. Moen, A. P. van Eyken, K. Oksavik, I. W. McCrea, and M. Lester (2005), Motion of the dayside polar cap boundary during substorm cycles: II. Generation of poleward-moving events and polar cap patches by pulses in the magnetopause reconnection rate, *Ann. Geophys.*, *23*, 3513–3532.
Malakit, K., M. A. Shay, P. A. Cassak, and C. Bard (2010), Scaling of asymmetric magnetic reconnection: Kinetic particle-in-cell simulations, *J. Geophys. Res.*, *115*, A10223, doi:10.1029/2010JA015452.
Milan, S. E., J. S. Gosling, and B. Hubert (2012), Relationship between interplanetary parameters and the magnetopause reconnection rate quantified from observations of the expanding polar cap, *J. Geophys. Res.*, *117*, A03226, doi:10.1029/2011JA017082.
Newell, P. T., T. Sotirelis, K. Liou, C.-I. Meng, and F. J. Rich (2007), A nearly universal solar wind-magnetosphere coupling function inferred from 10 magnetospheric state variables, *J. Geophys. Res.*, *112*, A01206, doi:10.1029/2006JA012015.
Otto, A. (2001), Geospace Environment Modeling (GEM) magnetic reconnection challenge: MHD and Hall MHD—Constant and current dependent resistivity models, *J. Geophys. Res.*, *106*, 3751–3757.
Parker, E. N. (1979), *Cosmical Magnetic Fields* Sect. 15.6, Clarendon Press, Oxford.
Phan, T. D., G. Paschmann, C. Twitty, F. S. Moser, J. T. Gosling, J. P. Eastwood, M. Oieroset, H. Reme, and E. A. Lucek (2007), Evidence for magnetic reconnection initiated in the magnetosheath, *Geophys. Res. Lett.*, *34*, L14104, doi:10.1029/2007GL030343.
Podolsky, B. (1947), On the Lorentz transformation of charge and current densities, *Phys. Rev.*, *72*, 624–626.
Pulkkinen, T. I., M. Palmroth, E. I. Tanskanen, N. Y. Ganushkina, M. A. Shukhtina, and N. P. Dmitrieva (2007), Solar wind—Magnetosphere coupling: A review of recent results, *J. Atmos. Sol. Terr. Phys.*, *69*, 256.
Rastatter, L., M. M. Kuznetsova, D. G. Sibeck, and D. H. Berrios (2012), Scientific visualization to study flux transfer events at the Community Coordinated Modeling Center, *Adv. Space Res.*, *49*, 1623.
Reiff, P. H., and J. G. Luhmann (1986), Solar wind control of the polar-cap voltage, in *Solar Wind-Magnetosphere Coupling*, edited by Y. Kamide and J. A. Slavin, p. 453, Terra Scientific, Tokyo, Japan.
Ren, Y., M. Yamada, H. Ji, S. Dorfman, S. P. Gerrhardt, and R. Kulsrud (2008), Experimental study of the Hall effect and electron diffusion region during magnetic reconnection in a laboratory plasma, *Phys. Plasmas*, *15*, 082,113.
Ridley, A. J. (2007), Alfven wings at Earth's magnetosphere under strong interplanetary magnetic fields, *Ann. Geophys.*, *25*, 533.

Rothwell, P. L., and J. R. Jasperse (2007), A coupled solar wind-magnetosphere-ionosphere model for determining the ionospheric penetration electric field, *J. Atmos. Sol. Terr. Phys.*, *69*, 1127.

Sergeev, V. A., and B. M. Kuznetsov (1981), Quantitative dependence of the polar cap electric field on the IMF $B_z$-component and solar wind velocity, *Planet. Space Sci.*, *29*, 205.

Seyler, C. E., Y. Salu, D. Montgomery, and G. Knorr (1975), Two-dimensional turbulence in invicid fluids or guiding center plasmas, *Phys. Fluids*, *18*, 803.

Shay, M. A., J. F. Drake, B. N. Rogers, and R. E. Denton (2001), Alfvenic collisionless magnetic reconnection and the Hall term, *J. Geophys. Res.*, *106*, 3759–3772.

Sonnerup, B. U. O. (1974), Magnetopause reconnection rate, *J. Geophys. Res.*, *79*, 1546–1549.

Swisdak, M., and J. F. Drake (2007), Orientation of the reconnection X-line, *Geophys. Res. Lett.*, *34*, L11106, doi:10.1029/2007GL029815.

Vassiliadis, D., A. J. Klimas, J. A. Valdivia, and D. N. Baker (1999), The Dst geomagnetic response as a function of storm phase and amplitude and the solar wind electric field, *J. Geophys. Res.*, *104*, 24,957–24,976.

Walsh, B. M., D. G. Sibeck, Y. Nishimura, and V. Angelopoulos (2013a), Statistical analysis of the plasmaspheric plume at the magnetopause, *J. Geophys. Res. Space Physics*, *118*, 4844–4851, doi:10.1002/jgra.50458.

Walsh, B. M., T. D. Phan, D. G. Sibeck, and V. M. Souza (2013b), The plasmaspheric plume and magnetopause reconnection, *Geophys. Res. Lett.*, doi:10.1002/2013GL058802.

Wygant, J. R., R. B. Torbert, and F. S. Mozer (1983), Comparison of S3-3 polar cap potential drops with the interplanetary magnetic field and models of magnetopause reconnection, *J. Geophys. Res.*, *88*, 5727–5735.

Yamada, M., Y. En, H. Ji, J. Beslau, S. Gerhardt, R. Kulsrud, and A. Kuritsyn (2006), Experimental study of two-fluid effects on magnetic reconnection in a laboratory plasma with variable collisionality, *Phys. Plasmas*, *13*, 052,119.